Asian Journal of Chemistry; Vol. 34, No. 9 (2022), 2357-2362

ASIAN JOURNAL OF CHEMISTRY

https://doi.org/10.14233/ajchem.2022.23886

Synthesis of Zinc Oxide Nanoparticles Employing *Costus igneus* Leaf Extract and their Antibacterial, Antifungal and Anticarcinogenic Activities

R. KAYALVIZHI[1], R. VIJAYASHANTHI[2], V. VIJAYA[3] and K. NEYVASAGAM[4,*]

[1]Department of Physics, E.M.G. Yadava Women's College (Affiliated to Madurai Kamaraj University), Madurai-625014, India
[2]Department of Physics, Parvathy's Arts and Science College, Dindigul-24002, India
[3]Department of Botany, E.M.G.Yadava Women's College, Madurai-625014, India
[4]Department of Physics, The Madura College, Madurai-625011, India

*Corresponding author: E-mail: r.kayalvizhi-phy@emgywomenscollege.ac.in; srineyvas@gmail.com

Received: 27 April 2022; *Accepted*: 30 June 2022; *Published online*: 19 August 2022; AJC-20934

An eco-friendly environment concerning the synthesis of nanoparticles from medicinal plants, free off or minimal usage of toxic chemicals is a requisite in the research avenues. Present study describes an environment-friendly green synthesis of ZnO nanoparticles acquired from leaf extracts of *Costus igneus* medicinal plant. The formation of ZnO with hexagonal Wurtzite structure is confirmed by XRD analysis and an average crystallite size was estimated as 30 nm. The UV absorbance investigation shows that the optical band gap value of ZnO nanoparticles is 3.25 eV. The ZnO nanoparticles smooth surface morphology, which was observed in SEM investigation. The EDAX study proved the occurrence of oxygen and zinc in the green synthesised nanoparticle. Effective antibacterial inhibition activity was observed against human bacterial species of (*E. coli*, *Pseudomonas aeruginosa*, *Staphylococcus aureus* and *Bacillus subtilis*) and then human fungal (*Aspergillus niger*, *Aspergillus flavus* and *Oidium caricae*). The cytotoxicity activity of breast cancer cells (MCF7) of IC_{50} was calculated as 59.14 µg/mL. Thus, the analysis of feasible herbal-based ZnO nanoparticles from *Costus igneus* leaf with significant repercussions can be exploited in the application of nanotechnology industries, biomedical and pharmaceutical drug preparations.

Keywords: Green synthesis, Zinc oxide nanoparticles, *Costus igneus*, Antimicrobial activity, Anticancer activity.

INTRODUCTION

Zinc oxide nanoparticles have attracted a lot of researchers attention because of its unique photocatalytic properties and numerous applications in optical [1], electrical [2], gas sensors [3], memory devices [4], photodiodes [5], photodetectors [6], dye-sensitized solar cells [7], textiles [8] and supercapacitors [9]. Green synthesis of zinc oxide nanoparticles from plant components like seed, roots, leaves, flowers, latex and stem bark have led to the progress of different approaches with direct applications in antibacterial, antifungal, antidiabetic, anticancer, wound dressings and modified textiles [10-15]. Zinc oxide nanoparticles have been synthesised from various plants leaf extract of *Aloe barbadensismiller* [16], *Catharanthus roses* [17], *Camellia sinesis* [18], *Ocimum basilicum* [19], *Plectranthus amboinicus* [20], *Pongamia pinnata* [21] and *Trifolium pratense* flower extract [22].

The Genus *Costus* is a vital meditative plant belonging to the family of *Costaceae*. The leaf of this plant helps to synthesize insulin in the human body, therefore referred to as the "insulin plant". The distinctive property of the insulin plant is used as a dietary supplement for the treatment of diabetes mellitus. Shiny *et al.* [23] showed that the phytochemicals like corosolic acid, terpenoids, saponins, flavonoids, sapogenin, tannins and steroids present in this plant helps to cure various diseases. The numerous medicinal values of the *Costus igneus* plant has been reported by researchers however research findings using this medicinal plant in green synthesis of ZnO nanoparticles is not studied. The objective of this work is to synthesize zinc oxide nanoparticles using *Costus igneus* plant leaves extract, to characterize its antimicrobial (human bacterial and fungal pathogens) and anticancer activity.

EXPERIMENTAL

Young *Costus igneus* leaves were picked from the garden and cleaned well with tap water before being rinsed with distilled water. The veins of the leaves were removed and sliced into

small sizes. Sliced leaves (100 g) were ground in pastelaria mortar, using double distilled water. Initially, the extract was screened *via* a nylon mesh and then through Whatman filter paper. The resulting filtrate was employed in further preparations of ZnO. Zinc acetate solution (20 mM of 80 mL) was incubated at 60 ºC (continuous stirring was followed throughout the experiment). After 1 h, 20 mL of leaf extract was poured and retained for another 0.5 h. To convert zinc acetate to zinc oxide, 400 mg of sodium hydroxide was added to the above combination. A light green precipitate formation confirmed the reduction reaction; it took 2 h for the complete reduction. The biosynthesized nanoparticles were centrifuged dried at 40 ºC and stored as a powder in the refrigerator for analysis.

Characterization: The optical characteristics of ZnO nanomaterials were investigated by recording absorption spectroscopy in the range 280-1100 nm with a (Ocean optics HR2000, USA) UV-Vis-NIR spectrophotometer. A Thermo Nicolet 380 FTIR spectrometer was used for the FTIR analysis, which was tuned to 4000-400cm^{-1} with a resolution of 0.5 cm^{-1} and a wavelength accuracy of 0.01 cm^{-1}. The study of XRD was carried out on a (X' Pert Pro-Panalytic) Powder X-Ray diffractometer that was functioned at 40 kV with a current of 30 mA under Cu*K*α rays with a 2θ between 10º and 80º, while the Tescan VEGA 3SBH was used to document SEM with EDAX images using a Bruker Easy EDS system with an applied potential of 0.3-30 kV.

Antimicrobial activity: The antimicrobial study was determined by the well diffusion method using Muller Hinton agar media [17]. Penicillin and cotrimoxazole were used as an antimicrobial standard. The test human bacterial pathogens (*Escherichia coli*, *Pseudomonas aeruginosa, Staphylococcus aureus* and *Bacillus subtilis*) and fungal pathogens (*Aspergillus niger*, *Aspergillus flavus* and *Oidium caricae*) were swabbed on the surface of plated agar. Test samples (25 µL) were impregnated in agar wells and permitted the compound to diffuse into the medium and later incubated at 30 ºC for 24 h. The diameters of the inhibitory zone were measured in millimetres. Each antimicrobial assay was carried out three times and an average values is reported.

Anticancer activity: The MTT treatment was used to investigate the *in vitro* cytotoxicity of ZnO nanopowder in MCF-7 cells [24]. Trypsinization was used to harvest MCF-7 cells, which were then aggregated in a 15 mL test tube. The cells were then seeded in a 96-well plate with a cell concentration of 1105 cells/well cells/mL (200 µL) for 24-48 h at 37 ºC in a DMEM solution comprising 1% antibiotic reagent and 10% FBS. The wells were cleaned with antiseptic PBS and incubated with different doses of ZnO nanopowder in a serum-free DMEM environment. Every cell specimen was examined in triplicate and cultivated for 24 h at 37 ºC in a cool and dry CO_2 incubator. MTT (20 µL of 5 mg/mL) was introduced to each well following the incubation time and the cells were cultured for further 2-4 h till violet precipitates were observable and confirmed using a microscope. Subsequently, the medium, along with MTT (220 µL), was evacuated from the wells and flushed with 1X PBS (200 µL); moreover, DMSO (100 µL) was applied to dissolve the generation of crystals and the dish was agitated for 5 min. Employing a microplate scanner (Thermo Fisher Scientific, USA), the absorption of every well was quantified at 570 nm and IC_{50} readings and the proportion of cell vitality were computed using USA software called graph Pad Prism 8.0.

RESULTS AND DISCUSSION

XRD characterization: The synthesized ZnO nanoparticles were analyzed using XRD to scrutinize the crystal phase, purity and crystallinity. The sharp diffraction peaks in XRD result reveals that the produced ZnO nanoparticles have well crystalline nature (Fig. 1). Miller planes (100), (002), (101), (102), (110), (103), (201), and (004) are ascribed to the diffraction peaks occurring at 2θ of 31.84º, 34.53º, 36.31º, 47.57º, 60.61º, 62.95º, 69.22º and 72.19º, respectively. The strong and narrow diffraction peaks, which imply a hexagonal Wurtzite crystallite structure, agree well with the powder ZnO data card from the standard JCPDS 36-1451. The mean crystalline size is 30 nm, according to Debye-Scherrer's formula:

$$D = \frac{0.94\lambda}{\beta\cos\theta}$$

where D refers to size of the crystallite, wavelength (1.5406 Å Cu*K*α) is represented by λ, full-width at half-maximum (FWHM) of predominant intensity peak is β in radians and diffraction angle is θ. The XRD patterns found in this investigation are similar to the XRD patterns as reported Suresh *et al.* [25].

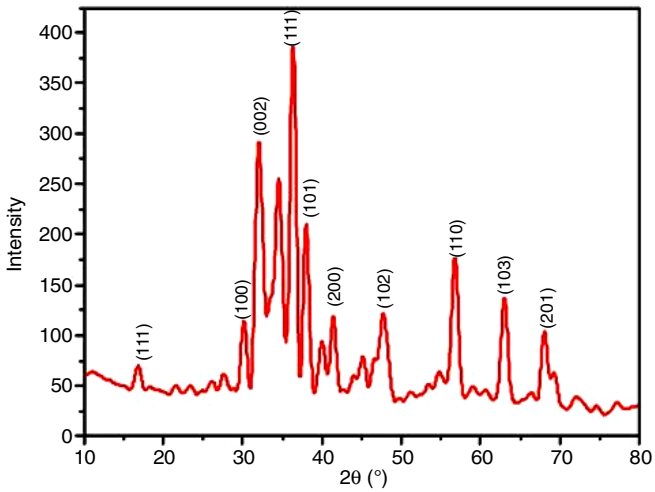

Fig. 1. XRD pattern of green synthesised ZnO nanoparticles

UV-Vis characterization: The UV-Vis absorbance spectroscopic result of ZnO nanocrystals is shown in Fig. 2a. The optical bandgap was calculated using Tauc's equation

$$\alpha h\nu = A\,(h\nu - E_g)^n$$

where α is the absorbance constants, E_g is the bandgap of the material, h indicates Planck's constant, ν is the frequency of incident light, and n is 2 and 1/2 for indirect and direct bandgap respectively. Tauc's plot reveals that the band gap of pure ZnO nanoparticles is 3.25 eV (Fig. 2b). Azizi *et al.* [26] also found comparable band gap values of ZnO nanoparticles synthesized from *C. pictus* extract.

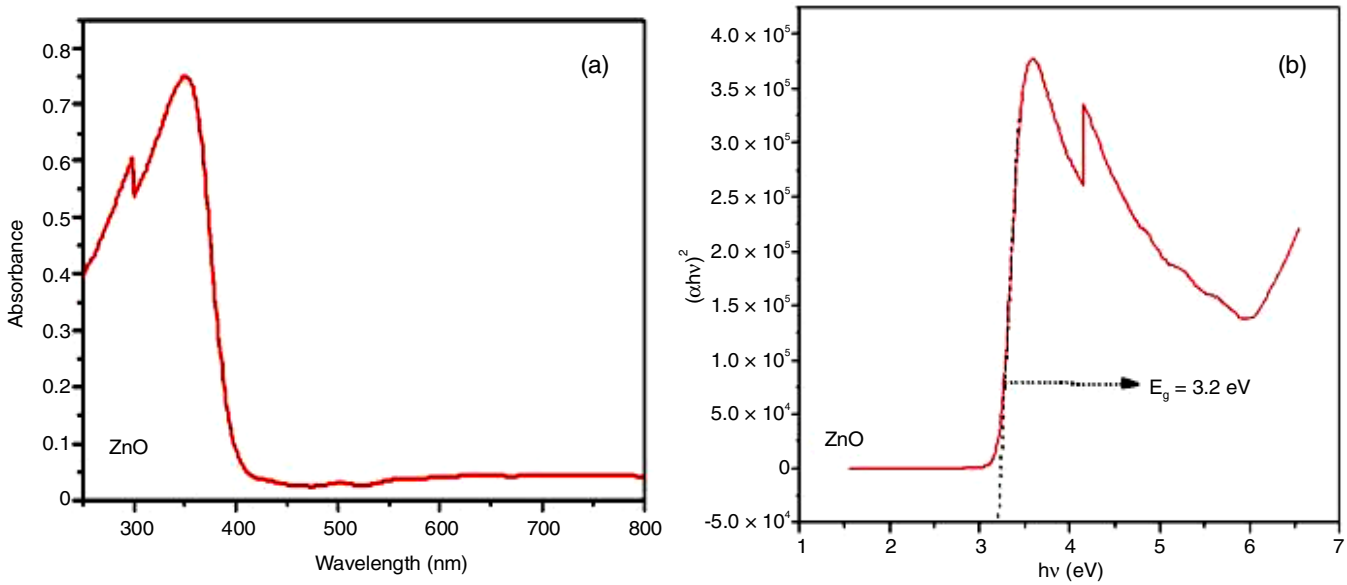

Fig. 2. (a) UV absorption spectrum of green synthesized ZnO nanoparticles (b) Tauc's plot of ZnO nanoparticles

FTIR characterization: FTIR spectrum of plant extract (Fig. 3a) revealed a broad range of 3408.95 cm^{-1} corresponding to O-H stretching vibration. A narrow peaks obtained at 1637.45 cm^{-1} and 1425.30 cm^{-1} indicate the C=C stretch alkane group and O-H bending an aliphatic carboxylic acid, respectively. A peak at 1027.02 cm^{-1} corresponds to C-N stretching vibrations. The bands appeared at 721.33 cm^{-1} and 669.25 cm^{-1} strongly depicting the presence of C=C bending alkene group and C-Br stretch alkyl halide. The FTIR study indicated that phenolic compounds in flavonoids bound to metal, to avoid clumping of metal nanoparticles and sustain ZnO in the solution [25]. This reveals that biological molecules play dual roles in the synthesis and stability of zinc oxide nanoparticles.

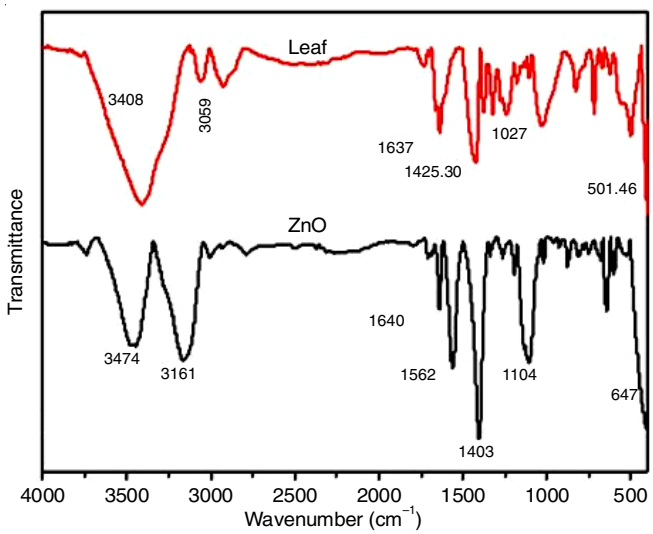

Fig. 3. FTIR spectra of *Costus igneus* plant leaf extract (a) and ZnO nanoparticles (b)

FTIR spectra and functional groups involved in the ZnO NPs (Fig. 3b) synthesis was illustrated as peaks in the range of 4000-500 cm^{-1} in Fig. 3. Wide peaks obtained at 3474.52 and 3161.11 cm^{-1} correspond to O-H and alkenyl C-H stretching vibrations. The sharp peaks obtained at 1562.23 and 1403.12 cm^{-1} show that the presence of aromatic C=C bending vibrations and O-H bending aliphatic carboxylic acid group. The peaks present in the spectrum range of 1104.17 cm^{-1} indicate C-O stretching vibrations. The intensity of absorption in the 525.57 cm^{-1} clearly indicates a hexagonal phase of ZnO. Santhosh Kumar *et al.* [27] observed that the existence of phenolic group and flavonoids in the extract of *Malva sylvestris* plant leaf increases the production and stability of ZnO nanoparticles.

Morphology characterization: Fig. 4 shows the SEM images of ZnO nanostructures that vividly show the granules are in the form sphere. These ZnO nanostructures are built by tiny nanocrystals with high uniformity and an average particle

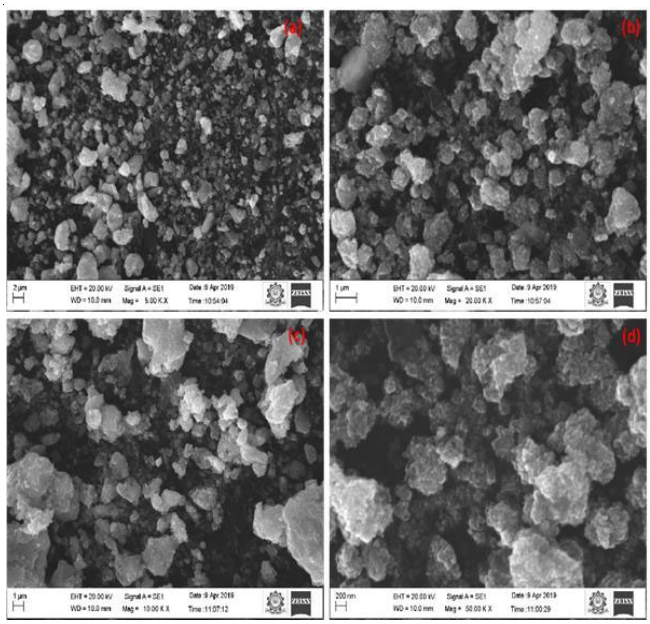

Fig. 4. SEM images of green synthesized ZnO nanoparticles

size of 5-30 nm. The same spherical shape of the zinc oxide nanostructures was reported by Shwetha *et al*. [28] and the average size was predicted to be 20-40 nm.

The EDAX study confirms the presence of zinc and oxygen in zinc oxide nanomaterials (Fig. 5). The presence of 83.8 % zinc and 16.2% oxygen in this elemental composition of the nanoparticles suggests that the synthesized ZnO nanocrystals are with high oxygen defaults, which are more helpful in all applications.

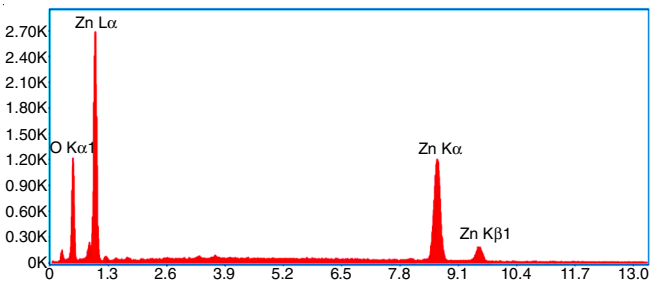

Fig. 5. EDAX spectrum of green synthesized ZnO nanoparticles

Biological activity of ZnO nanoparticles: The process of physical interaction among bacteria and metal nanoparticles is responsible for the green production of ZnO nanoparticles towards bacterial cells [29,30]. The simultaneous generation of radical oxygen species (ROS), the discharge of Zn^{2+} and the cationic characteristics of ZnO nanoparticles pierce the negative charge of the cell membrane and destroy the bacteria (*E. coli*, *B. subtilis, S. aureus* and *P. aeruginosa*) and fungal cells (*O.caricae*, *A. niger* and *A. flavus*) resulting in protein, genetic material and mineral spillage [31]. The nanoparticles of smaller sizes exhibit higher reactivity by increasing their efficacy of antimicrobial activity related to the nanoparticles of larger sizes [30].

The results have been analyzed by measuring the microbial zone of inhibition among different bacterial and fungal strains. Table-1 shows the antibacterial activity investigated towards Gram-negative and Gram-positive bacterial strains (*E. coli*, *B. subtilis, S. aureuss* and *P. aeruginosa*) and used levoflaxin as a standard. The biosynthesized ZnO nanopowder revealed exquisite antibacterial performance. In comparison, *B. subtilis* shows the greater inhibitory zone (23mm) followed by *P. aeruginosa* (22 mm), *S. aureus* (21 mm) and *E. coli* (19 mm). The green synthesized ZnO nanoparticles from *Costus igneus* leaf extract showed high antibacterial efficacy towards both Gram-positive and Gram-negative bacteria pathogens when compared to the conventional levoflaxin. A similar observation was done in ZnO nanoparticles from *Catharanthus roseus* leaf extract against *K. pneumonia*, *S. aureus*, *E. coli* and *Bacillus* studied by Bhumi & Savithramma [17]. The electrostatic coupling among negatively charged microbial cell membranes and positively charged nanocrystals is thought to be responsible for antimicrobial effectiveness [31].

Table-2 shows the antifungal activity of biosynthesized ZnO nanoparticles against three fungal strains (*A. flavus*, *O. caricae* and *A. niger*). As compared to the standard cotrimoxazole, the zone of inhibition of the experimental organism shows less

TABLE-1
ANTIBACTERIAL RESULT FOR THE
GREEN SYNTHESIZED ZnO NANOPARTICLES

Bacterial strains	Zone of inhibition in diameter (mm)		
	Control-isopropanol	Levofloxacin	ZnO
E. coli	No zone	13	19
Pseudonomonas aeruginosa	No zone	11	22
Staphylococcus aureus	No zone	14	21
Bacillus subtilis	No zone	29	23

TABLE-2
ANTIFUNGAL RESULT FOR THE
GREEN SYNTHESIZED ZnO NANOPARTICLE

Fungus	Zone of inhibition in diameter (mm)		
	Control-isopropanol	Cotrimoxazole	ZnO
Odiumcaricae	No zone	21	8
Aspergillus flavus	No zone	15	9
Aspergillus niger	No zone	33	No zone

antifungal efficacy. The zone of inhibition observed in *A. flavus* is 9 mm and *O. caricae* is 8 mm and the antifungal activity is nill in *A. niger*. The findings of the present study suggested that the fungal cell wall is highly resistant to the green synthesized ZnO nanoparticles of *C. Igneus* leaf extract. Further analysis of increasing the concentration of synthesized nanoparticles against the fungal strains study is essential. Rajiv *et al*. [32] reported on similar findings of biosynthesized of zinc oxide nanocrystals employing leaf extract of *P. hysterophorus* L. and their size-dependent antifungal efficacy. Comparatively, the synthesized ZnO nanoparticles of the present study has greater efficacy towards bacterial (*E. coli*, *B. subtilis*, *S. aureus* and *P. aeruginosa*) than the fungal cells (*O. caricae*, *A. niger* and *A. flavus*).

Anticancer analysis: The MTT experiment was used to analyzed the anticancer efficacy of ZnO nanoparticles made from *C. igneus* leaf extract towards MCF-7 breast carcinoma cell variants [33]. Fig. 6 indicates that plotting of cell survival viability *versus* drug concentration (µg/mL) was used to calculate the cell growth inhibition (IC_{50}). The graph shows that dosage dependent decreases in cellular viability while the synthesized nanoparticle concentration increases. The IC_{50} for ZnO NPs was determined to be 59.14 µg/mL. Shwetha *et al*. [28] observed that the synthesized ZnO nanoparticles using *Areca catechu* leaves extract IC_{50} was found to be 52.64 µg/ml. The optical density is proportional to the cellular viability, is shown in Fig. 7. The OD value at 570 nm was calculated for different concentrations of ZnO nanoparticles 0, 5, 10, 15, 50, 100, 200, 300, 400 and 500 µg/mL. The results showed that an increase in the concentration of ZnO nanoparticles increases the optical density value and attains a mean value of 0.373 nm.

The cytotoxic effects of ZnO nanoparticles on MCF-7 cell lines treated with different concentrations from 1, 5, 10, 15, 50, 100, 200, 300, 400 and 500 µg/mL, with a decrease in cell viability of 100, 97.85, 90.7, 85.34, 66.84, 70.86, 66.21, 54.86, 41.73, 32.25 and 28.86 respectively was observed. Guruviah *et al*. [24] investigated the cytotoxic effects of GS-ZnO nanoparticles in MCF-7 cell lines treated with doses

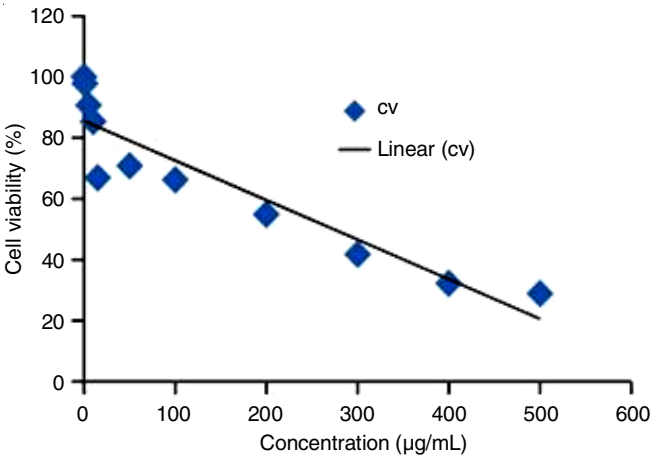

Fig. 6. Cell survival viability *versus* drug concentration (µg/mL)

of 0, 25, 62.5, 125, 250, 500, 750 and 1000 µg/mL and found that cell viability was less at 100, 85.21, 67.38, 42.03, 13.69, 2.01, 1.30, 1.01, respectively lesser in percentage. The illustration strongly demonstrates that raising the quantity of nanoparticles in the cell suspension, resulting in numerous nanoparticles attacking the cell walls (Fig. 8), can contribute to an upsurge

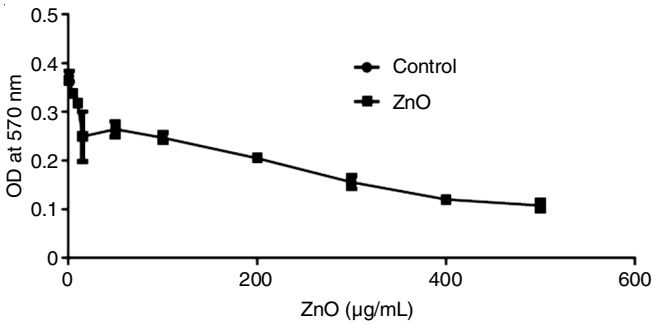

Fig. 7. Optical density against various concentrations of green synthesized ZnO nanoparticles

in the number of destroying cellular organs and ultimately, death of cancer cells. Selvakumari *et al*. [33] also studied ZnO nanoparticles from 7.8 µg/mL to 31.2 µg/mL concentration the cell viability percentage significantly reduced from 82.8 to 50.8 (MCF7).

Conclusion

Costus igneus leaf extract was used as a reducing agent in the green production of ZnO nanoparticles. The XRD, UV, FTIR, SEM, EDX, antibacterial and anticancer analyses were

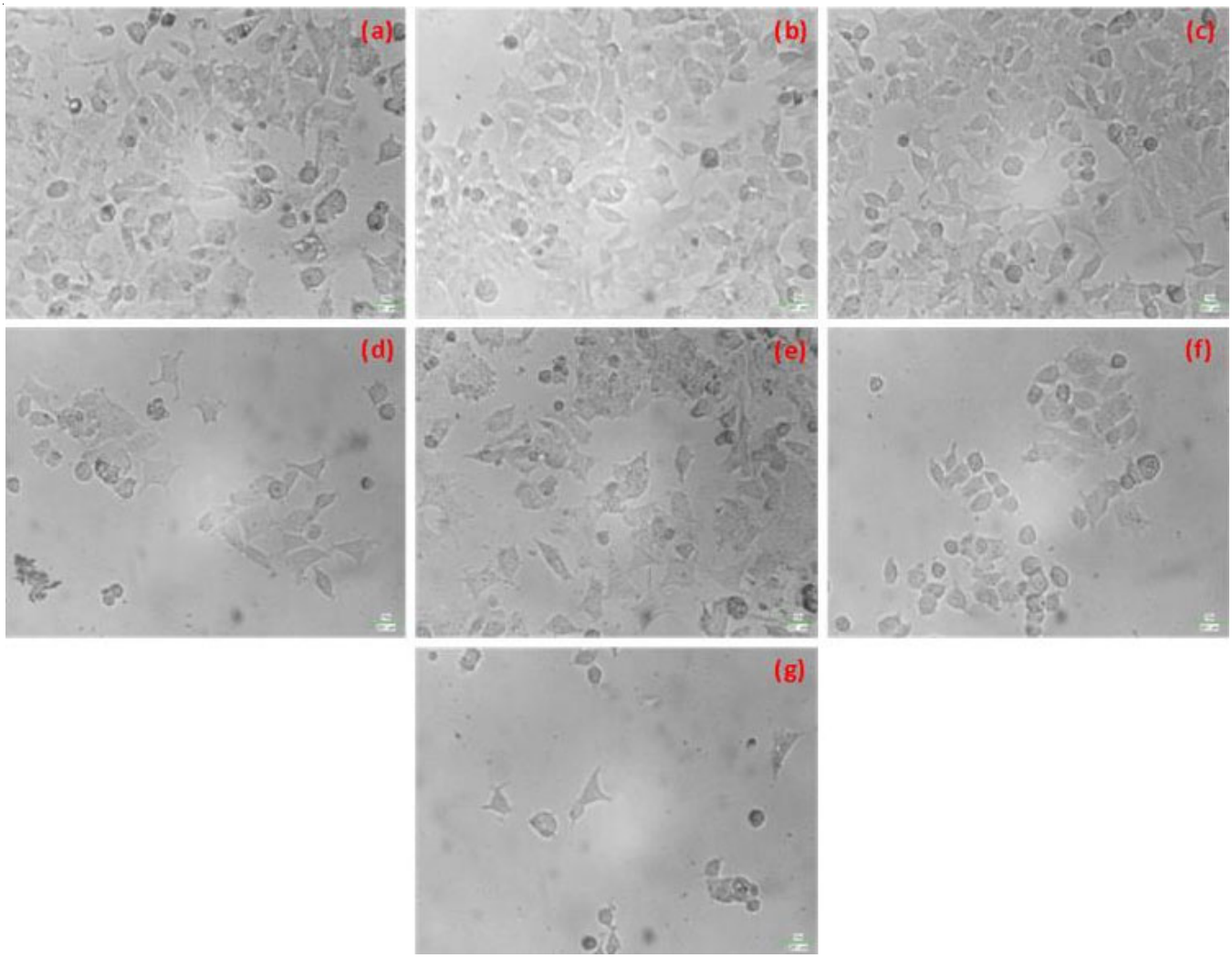

Fig. 8. Anticancer images of ZnO nanoparticles: (a) control, (b) 1 µg, (c) 10 µg, (d) 50 µg, (e) 100 µg, (f) 300 µg and (g) 500 µg

studied to confirm the successful synthesis of ZnO nanoparticles. The average crystallite size observed from the plane was 30 nm, according to XRD measurements. The bandgap energy of ZnO nanoparticles calculated from the UV graph is 3.25 eV. The existence of functional groups of ZnO nanostructures was verified in the FTIR spectrum. In SEM, the typical particle image size was 5-30 nm. The occurrence of ZnO complexes is confirmed by the EDAX. Antibacterial action was found in the green produced ZnO nanoparticles towards *B. subtilis*, *E. coli*, *S. aureus* and *P. aeruginosa* as well as stronger antifungal efficacy was observed against *A. flavus*. The cytotoxic effects of ZnO nanoparticles toward MCF-7 cells have been evaluated in various concentrations and exhibited dosage-dependent inhibition against the proliferation of breast cancer cell lines. Thus, certain human bacterial and fungal infections were discovered to be protected by ZnO nanoparticles, hinting that they might be used in biomedical applications as an efficient antibacterial and anticancer medicines.

CONFLICT OF INTEREST

The authors declare that there is no conflict of interests regarding the publication of this article.

REFERENCES

1. C. Belkhaoui, N. Mzabi, H. Smaoui and P. Daniel, *Results Phys.*, **12**, 1686 (2019); https://doi.org/10.1016/j.rinp.2019.01.085
2. A. Zankat, H. Boricha, S. Solanki, K. Sagapariya, M. Gal, V.S. Vadgama, P.S. Solanki, N.A. Shah and D.D. Pandya, *Mater. Today Proc.*, **17**, 1 (2019); https://doi.org/10.1016/j.matpr.2019.06.394
3. V.S. Bhati, M. Hojamberdiev and M. Kumar, *Energy Rep.*, **6**, 46 (2020); https://doi.org/10.1016/j.egyr.2019.08.070
4. N.M. Muhammad, N. Duraisamy, K. Rahman, H.W. Dang, J. Jo and K.H. Choi, *Curr. Appl. Phys.*, **13**, 90 (2013); https://doi.org/10.1016/j.cap.2012.06.017
5. S.S. Mousavi, B. Sajad and M.H. Majlesara, *Mater. Des.*, **162**, 249 (2019); https://doi.org/10.1016/j.matdes.2018.11.037
6. K. Charipar, H. Kim, A. Piqué and N. Charipar, *Nanomaterials*, **10**, 1648 (2020); https://doi.org/10.3390/nano10091648
7. R. Shashanka, H. Esgin, V.M. Yilmaz and Y. Caglar, *J. Sci.: Adv. Mater. Devices*, **5**, 185 (2020); https://doi.org/10.1016/j.jsamd.2020.04.005
8. A. Becheri, M. Dürr, P. Lo Nostro and P. Baglioni, *J. Nanopart. Res.*, **10**, 679 (2008); https://doi.org/10.1007/s11051-007-9318-3
9. M.S. Yadav, N. Singh and A. Kumar, *J. Mater. Sci. Mater. Electron.*, **29**, 6853 (2018); https://doi.org/10.1007/s10854-018-8672-5
10. G. Sundaraselvan and S.D. Quine, *J. Nanosci. Technol.*, **3**, 289 (2017).
11. L.F.A. Raj and E. Jayalakshmy, *Orient. J. Chem.*, **31**, 51 (2015); https://doi.org/10.13005/ojc/310105
12. S.K. Chaudhuri and L. Malodia, *Appl. Nanosci.*, **7**, 501 (2017); https://doi.org/10.1007/s13204-017-0586-7
13. P. Ramesh, A. Rajendran and M. Meenakshisundaram, *J. Nanosci. Nanotechnol.*, **2**, 41 (2014).
14. M.S. Geetha, H. Nagabhushana and H.N. Shivananjaiah, *Mater. Today Proc.*, **5**, 22328 (2018); https://doi.org/10.1016/j.matpr.2018.06.599
15. H. Umar, D. Kavaz and N. Rizaner, *Int. J. Nanomedicine*, **14**, 87 (2018); https://doi.org/10.2147/IJN.S186888
16. G. Sangeetha, S. Rajeshwari and R. Venckatesh, *Mater. Res. Bull.*, **46**, 2560 (2011); https://doi.org/10.1016/j.materresbull.2011.07.046
17. G. Bhumi and N. Savithramma, *Int. J. Drug Dev. Res.*, **6**, 208 (2014).
18. R.K. Shah, F. Boruah and N. Parween, *Int. J. Curr. Microbiol. Appl. Sci.*, **4**, 444 (2015).
19. H. Abdul Salam, R. Sivaraj and R. Venckatesh, *Mater. Lett.*, **131**, 16 (2014); https://doi.org/10.1016/j.matlet.2014.05.033
20. L. Fu and Z. Fu, *Ceram. Int.*, **41**, 2492 (2015); https://doi.org/10.1016/j.ceramint.2014.10.069
21. M. Sundrarajan, S. Ambika and K. Bharathi, *Adv. Powder Technol.*, **26**, 1294 (2015); https://doi.org/10.1016/j.apt.2015.07.001
22. R. Dobrucka and J. Dlugaszewska, *Saudi J. Biol. Sci.*, **23**, 517 (2016); https://doi.org/10.1016/j.sjbs.2015.05.016
23. C. Shiny, A. Saxena and S.P. Gupta, *Int. J. Pharm. Biomed. Res.*, **4**, 97 (2013).
24. K. Guruviah, S.K. Annamalai, A. Ramaswamy, C. Sivasankaran, S. Ramasamy, H. Barabadi and M. Saravanan, *Nanomed. J.*, **7**, 272 (2020); https://doi.org/10.22038/nmj.2020.07.00003
25. J. Suresh, G. Pradheesh, V. Alexramani, M. Sundrarajan and S.I. Hong, *Adv. Nat. Sci.: Nanosci. Nanotechnol.*, **9**, 015008 (2018); https://doi.org/10.1088/2043-6254/aaa6f1
26. S. Azizi, M.B. Ahmad, F. Namvar and R. Mohamad, *Mater. Lett.*, **116**, 275 (2014); https://doi.org/10.1016/j.matlet.2013.11.038
27. J. Santhoshkumar, S.V. Kumar and S. Rajeshkumar, *Resource-Efficient Technologies*, **3**, 459 (2017); https://doi.org/10.1016/j.reffit.2017.05.001
28. U.R. Shwetha, M.S. Latha, C.R. Rajith Kumar, M.S. Kiran and V.S. Betageri, *J. Inorg. Organomet. Polym. Mater.*, **30**, 4876 (2020); https://doi.org/10.1007/s10904-020-01575-w
29. H.M. Yusof, R. Mohamad, U.H. Zaidan and N.A.A. Rahman, *J. Anim. Sci. Biotechnol.*, **10**, 57 (2019); https://doi.org/10.1186/s40104-019-0368-z
30. A. Sirelkhatim, S. Mahmud, A. Seeni, N.H.M. Kaus, L.C. Ann, S.K.M. Bakhori, H. Hasan and D. Mohamad, *Nano-Micro Lett.*, **7**, 219 (2015); https://doi.org/10.1007/s40820-015-0040-x
31. S.H.S. Dananjaya, R.S. Kumar, M. Yang, C. Nikapitiya, J. Lee and M. De Zoysa, *Int. J. Biol. Macromol.*, **108**, 1281 (2018); https://doi.org/10.1016/j.ijbiomac.2017.11.046
32. P. Rajiv, S. Rajeshwari and R. Venckatesh, *Spectrochim. Acta A Mol. Biomol. Spectrosc.*, **112**, 384 (2013); https://doi.org/10.1016/j.saa.2013.04.072
33. D. Selvakumari, R. Deepa, V. Mahalakshmi, P. Subhashini and N. Lakshminarayan, *ARPN J. Eng. Appl. Sci*, **10**, 5418 (2015).